IMPLEMENTATION OF THE ATLAS-SUSY-2018-04 ANALYSIS IN THE MADANALYSIS 5 FRAMEWORK

JONGWON LIM

Department of Physics, Hanyang University, Seoul 04763, Republic of Korea

CHIH-TING LU

School of Physics, KIAS, Seoul 02455, Republic of Korea

JAE-HYEON PARK

School of Physics, KIAS, Seoul 02455, Republic of Korea

JIWON PARK

Department of Physics, Hanyang University, Seoul 04763, Republic of Korea

We present the MADANALYSIS 5 implementation and validation of the ATLAS-SUSY-2018-04 search. This ATLAS analysis targets direct stau production in events with two hadronic tau leptons, and probes 139 fb^{-1} of LHC proton-proton collisions at a center-of-mass energy of 13 TeV. The validation of our reimplementation relies on a comparison of our cutflow predictions with the auxiliary material and official results provided by the ATLAS collaboration in the context of two supersymmetry-inspired simplified benchmark models in which the Standard Model is extended by a neutralino and a stau decaying into a tau lepton and a neutralino. Add some quantitative statement about the obtained level of agreement. The recasting results agree with ATLAS cutflow at the level of 6-8% in heavy stau scenario, and increase to 15-50% in light stau scenario due to large discrepancies from one of the kinematic cut.

1. Introduction

In this note, we describe the validation of the implementation, in the MADANALYSIS 5 framework,[1–4] of the ATLAS-SUSY-2018-04 search[5] for direct stau production in events featuring two hadronic tau leptons and a large amount of missing transverse energy (E_T^{miss}). This analysis focuses on LHC proton-proton collisions at a center-of-mass energy of 13 TeV, and considers an integrated luminosity of 139fb^{-1}. The typical supersymmetric signal which this analysis is dedicated to is illustrated by the representative Feynman diagram shown in Fig. 1.

For the validation of our reimplementation, we have focused on a simplified model in which only a few electroweakly-interacting superpartners are relevant.

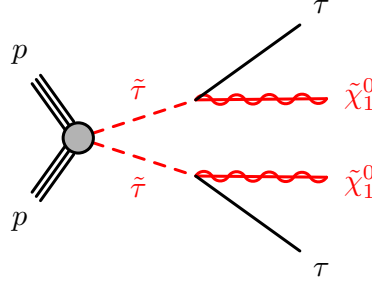2 *Jongwon Lim, Chih-Ting Lu, Jae-hyeon Park and Jiwon Park*

Fig. 1. The Feynman diagram for the process $pp \to \tilde{\tau}\tilde{\tau} \to \tilde{\chi}_1^0\tilde{\chi}_1^0\tau\tau$.

The lightest neutralino ($\tilde{\chi}_1^0$) is taken as the lightest supersymmetric particle (LSP). The stau-left ($\tilde{\tau}_L$) and stau-right ($\tilde{\tau}_R$) sleptons are moreover assumed to be mass degenerate and they do not mix. Therefore the gauge eigenstates ($\tilde{\tau}_L$,$\tilde{\tau}_R$) coincide with the mass eigenstates ($\tilde{\tau}_1$,$\tilde{\tau}_2$) in this theoretical framework. Furthermore, in order to suppress any other decay modes of the tau sleptons, the masses of all charginos and neutralinos are set to 2.5 TeV except for the $\tilde{\chi}_1^0$ neutralino. Hence, the single kinematically allowed decay mode of the staus is

$$\tilde{\tau} \to \tilde{\chi}_1^0\tau \qquad (1)$$

Finally, all squarks, that do not contribute at leading-order, are decoupled as well. Add a paragraph detailing the content of the note: in Sec. X, we present... Sec. Y is dedicated to... *etc.* This note is organized as follows. In Sec. 2, we present outline of the analysis, followed by definition of physics objects and event selections implemented for recasting. Sec. 3 is dedicated to the generation of events and comparison of recasting and ATLAS official results. In Sec. 4, we summarize our work.

2. Description of the analysis

This analysis targets a final state containing two hadronic tau leptons with a certain amount of missing transverse energy. The kinematics of the di-$\tau + E_T^{miss}$ system is used to reduce the contributions from Standard Model backgrounds. In Sec. 2.1, we first detail how the objects relevant for the analysis are reconstructed and defined. Then, in Sec. 2.2, we discuss the sequence of event selections that are applied in the aim of unravelling the signal from the background.

2.1. *Object definitions*

Jets are reconstructed by means of the anti-k_t algorithm[7] with a radius parameter set to $R = 0.4$. This analysis focuses on jets whose transverse momentum p_T^j and pseudorapidity η^j fullfill

$$p_T^j > 20 \text{ GeV} \quad \text{and} \quad |\eta^j| < 2.8. \qquad (2)$$

Moreover, the selected jets that are tagged as originating from the fragmentation of a b-quark must satisfy the stronger requirements

$$p_T^b > 20 \text{ GeV} \quad \text{and} \quad |\eta^b| < 2.5. \tag{3}$$

In the considered analysis, a b-tagging working point with an average efficiency of 77% is used. This working point corresponds to c-jet and light-jet rejection rates of 4.9 and 110, respectively.

Electron candidates are required to have a transverse momentum p_T^e and pseudorapidity η^e obeying

$$p_T^e > 17 \text{ GeV} \quad \text{and} \quad |\eta^e| < 2.47. \tag{4}$$

Furthermore, all electron candidates are required to have both track and calorimeter isolations. The condition of the track isolation is

$$\sum p_{T,\text{tracks}}/p_T^e < 0.15 \quad \text{with} \quad \Delta R = \min(10 \text{ GeV}/p_T^e, 0.2), \tag{5}$$

the condition of the calorimeter isolation is

$$\sum E_{T,\text{calorimeter}}/p_T^e < 0.2 \quad \text{with} \quad \Delta R = 0.2, \tag{6}$$

and for high transverse momentum electron, we use instead of the two above conditions

$$\sum E_{T,\text{tracks}} < max(0.015 \times p_T^e, 3.5 \text{ GeV}) \quad \text{with} \quad \Delta R = 0.2 \quad \text{if} \quad p_T^e > 200 \text{ GeV}. \tag{7}$$

Muon candidate definition is similar, although with slightly looser thresholds,

$$p_T^\mu > 14 \text{ GeV} \quad \text{and} \quad |\eta^\mu| < 2.7, \tag{8}$$

The condition of the track isolation is

$$\sum p_{T,\text{tracks}}/p_T^\mu < 0.15 \quad \text{with} \quad \Delta R = \min(10 \text{ GeV}/p_T^\mu, 0.3), \tag{9}$$

and the condition of the calorimeter isolation is

$$\sum E_{T,\text{tracks}}/p_T^\mu < 0.3 \quad \text{with} \quad \Delta R = 0.2. \tag{10}$$

In the ATLAS experiment, hadronically decaying tau lepton (τ_{had}) candidates are reconstructed with one or three associated charged pion tracks (prongs). For 1-prong (3-prong) τ lepton candidates, the signal efficiencies are 75% and 60% for the *medium* working point respectively. In the recasting based on MADANALYSIS 5 that we implement in this work, the simulation of the detector response is performed with the DELPHES 3[15] software. We consider a tau-tagging efficiency of 100% with a misidentification probability of 0% at the level of DELPHES 3, and handle medium and tight tau-tagging efficiencies through event reweighting factors extracted from the official ATLAS cutflow tables. Those factors are evaluated and included at the level of the analysis. Further details are given in Sec. 2.2.

Baseline tau lepton candidates are required to have

$$p_T^\tau > 50 \text{ (40) GeV} \quad \text{and} \quad |\eta^\tau| < 2.5 \tag{11}$$

for the leading (subleading) candidates, and the transition region between the barrel and endcap calorimeters ($1.37 < |\eta^\tau| < 1.52$) is excluded.

The object definition ends with some overlap removal conditions. The latter are implemented consistently to the analysis code provided through HEPData.[6] Tau leptons are removed if they are too close to an electron or a muon, with $\Delta R(\tau, e/\mu) < 0.2$. Electrons are then removed if they are too close to a muon, with $\Delta R(e, \mu) < 0.01$. Next, the jet collection is cleaned from those jets lying at an angular distance $\Delta R(j, e/\mu) < 0.2$ of a muon or an electron, and the electrons and muons that are too close to any of the remaining jets are removed if $\Delta R(e/\mu, j) < 0.4$. Finally, jets are removed if they are too close to one of the tau lepton candidates, with $\Delta R(j, \tau) < 0.4$.

2.2. *Event selection*

The next paragraphs should be clarified. There are so many reweighting factors... I would introduce the section by 2-3 sentences listing the different reweighting factors that will be considered, and the continue with the paragraphs describing all of them. Because DELPHES utilizes simplified and parametrized approaches to the detector simulation, it is hard to emulate detailed cut steps used in the real analysis. Firstly, several corrections are introduced as reweighting to mimic a trigger efficiency of ATLAS analysis. Also, to follow several stages of tau tagging selections presented in the analysis, additional reweighting factors are computed from official ATLAS results and applied to MADANALYSIS 5 implementation for *medium* and *tight* tau lepton cuts.

After the object definitions introduced in the previous subsection, events with exactly two baseline tau leptons are selected. All events are required to pass either an *asymmetric di-τ* trigger for the low stau mass region (SR-lowMass) or a combined *di-$\tau + E_T^{miss}$* ($E_T^{miss} > 150$ GeV) trigger for the high stau mass region (SR-highMass). This is coined *trigger and offline cuts* below. A trigger efficiency of 80% is applied in our recasting, after that we impose that the transverse momenta of the two leading tau candidates are larger than the offline p_T thresholds given in Table 1. Please give information on how the code selects which trigger cuts should be used (2018 or 2015-2017)-done To deal with different kinematic cuts for tau candidates in 2015-2017 and 2018 data taking period, corresponding fraction of events are randomly selected. A probability of imposing thresholds for 2018 dataset is calculated by the ratio of integrated luminosity of 2018 data among 139fb^{-1}.

Moreover, we assume that the tau leptons which fired the triggers are those selected through the offline cuts. A trigger-level τ_{had} identification efficiency for a tau candidate passing offline selection is set to 0.9 and applied for each tau lepton, in order to mimic medium tau identification procedure.[17] This leads to a total trigger reweighting factor of 64.8% that includes a global trigger efficiency of 80% and individual tau reconstruction efficiencies of 90%. (0.9 is P(offline&online | offline medium))

Table 1. Offline p_T thresholds for the leading (subleading) tau lepton candidate, in the case of the *asymmetric di-τ* (second column) and *di-τ* + E_T^{miss} (third column) triggers. This corresponds to a ditau efficiencies of about 80%.

Year	*asymmetric di-τ*	*di-τ* + E_T^{miss}
2015-2017	95 (60) GeV	50 (40) GeV
2018	95 (75) GeV	75 (40) GeV

After the handling of the triggers described above, events with exactly two *medium* tau lepton candidates with opposite-sign (OS) electric charges are selected. To treat the efficiency of selecting two offline mediumly tagged OS taus on top of a *di-tau(+E_T^{miss})* trigger selection (as DELPHES does not simulate charge misidentification), an additional event reweighting factor of 0.7 is enforced. This number is evaluated from the average ratio of the cut efficiencies provided by the ATLAS collaboration and those predicted by MADANALYSIS 5 when the identification of two medium taus is not included at the cutflow step called *2 medium τ (OS) and 3rd medium τ veto* below. (0.7 is the ratio of (ATLAS cut eff) / (MA5 cut eff but only OS condition is applied). Even though there's no charge misid in delphes, still small background taus exist. Since tau charge is taken from jet's charge, it is due to jet charge misid? The eff. only with OS cut is 93-94%)

In the next selection steps, a *b*-jet veto is enforced to reject events originating from top quark processes. Also, events featuring any additional light leptons (muons or electrons) are rejected. Finally, selection cuts common to both signal regions also include constraints on the reconstructed invariant mass of the two leading tau lepton system, $m(\tau_1, \tau_2)$. The latter is required to be larger than 120 GeV, in order to remove events exhibiting a pair of tau leptons stemming from low-mass resonances, Z boson, and Higgs boson decays (Z/H veto).

In the SR-lowMass region, a missing energy constraint of 75 GeV < E_T^{miss} < 150 GeV is imposed to increase the signal sensitivity. Moreover, the two selected tau leptons are required to be tight tagged. The selection efficiency p_{tight} associated with two *medium* taus passing the *tight* working point requirements is extracted from the official ATLAS cutflow tables. We rely on the ratio of the number of surviving weighted events before applying the tight tau lepton requirement, and after applying it. We use $p_{tight} \simeq 0.70$.

In the SR-highMass region, the tight tagging efficiency is extracted similarly, with the exception that at least one of two tau leptons should pass the tight selection requirements 9and not both of them). We use here $p_{tight} + 2\sqrt{p_{tight}}(1 - \sqrt{p_{tight}}) \simeq 0.91$.

The *stransverse mass m_{T2}* variable[18,19] [please add these two references - done] is defined as

$$m_{T2} = min_{\mathbf{q_T}} \left[max(m_{T,\tau_1}(\mathbf{p}_{T,\tau_1}, \mathbf{q}_T), m_{T,\tau_2}(\mathbf{p}_{T,\tau_2}, \mathbf{p}_T^{miss} - \mathbf{q}_T)) \right], \qquad (12)$$

6 *Jongwon Lim, Chih-Ting Lu, Jae-hyeon Park and Jiwon Park*

where $\mathbf{p}_{T,\tau_1}$ and $\mathbf{p}_{T,\tau_2}$ are the transverse momenta of the two tau lepton candidates. The transverse momentum vector of one of the invisible particle, $\mathbf{q}_T$, is choosen to minimize the larger of the two transverse mass m_{T,τ_1} and m_{T,τ_2}. The transverse mass m_T is defined by

$$m_T(\mathbf{p}_T, \mathbf{q}_T) = \sqrt{2(p_T q_T - \mathbf{p}_T \cdot \mathbf{q}_T)}. \tag{13}$$

In MADANALYSIS 5, the m_{T2} calculation can be done automatically through the function `PHYSICS->Transverse->MT2(vec1,vec2,ETmiss,Minvisible)`. In this expression, `vec1` and `vec2` stand for the two visible momenta, `ETmiss` for the miissing transverse momentum and `Minvisible` for a test mass that should map the expected mass of the invisible state.

A lower bound on the m_{T2} variable of 70 GeV is imposed, in order to reduce the contamination from $t\bar{t}$ and WW events. Finally, the two tau lepton candidates are required to be well separated in the transverse plane, by $\Delta R(\tau_1, \tau_2) < 3.2$ and $|\Delta\phi(\tau_1, \tau_2)| > 0.8$ to further suppress the contributions of the Standard Model backgrounds.

3. Validation

3.1. *Event generation*

In order to validate our analysis, we rely on the MSSM implementation[8] available in the FEYNRULES[9] model database and shipped with thew MAD-GRAPH5˙AMC@NLO event generator[10] as a UFO library.[20]Add the generic UFO reference.-done

We consider two benchmark points with masses $m(\tilde{\tau}, \tilde{\chi}_1^0) = (120, 1)$ GeV and $(280, 1)$ GeV to illustrate the validation of our reimplementation, as those correspond two scenarios for which official ATLAS cutflows and differential distributions are provided. The stau mixing matrix is additionally set to a unity matrix, so that the stau mass-eigenstates correspond to the right-handed and left-handed stau flavor-eigenstates.

We make use of MADGRAPH5 aMC@NLO version 2.6.7[10] for hard-scattering event generation for each of the two stau eigenstates, in which we convolute leading-order matrix elements with the NNPDF23LO[11] set of parton distribution function. Fix the NNPDF reference.-done Our signal matrix elements include the potential emission of up to two additional partons, and the different contributions are merged according to the MLM scheme.[12,13] We use a merging scale defined through the hard-scattering level parameter of MADGRAPH5˙AMC2NLO `xqcut` $= m_{\tilde{\tau}}/4$.

The PYTHIA package version 8.244[21] with the so-called $A14$ tune[22] has been used for the simulation of parton showering and hadronization. Fix the pythia reference and add an A14 reference-done. The simulation of the detector response has been performed by using DELPHES 3.4.2,[15] that relies on FASTJET[16] for object reconstruction.

We have tuned the ATLAS detector parameterization in DELPHES 3 appropriately, according to the needs of the analysis. For example, loosened isolation criteria are applied so that isolation could be implemented fully at the analysis level. Moreover, the radius parameter and minimum transverse momentum used for jet reconstruction are reduced to 0.4 and 15 GeV respectivey, and we have updated the *b*-tagging and tau-tagging performance. Finally, the `UniqueObjectFinder` module has been disabled as object overlap removal has been implemented at the level of the analysis.

3.2. *Comparison with the official results*

In Tables 2 and 3, we compare predictions obtained with our implementation to the official results provided in the form of auxiliary tables by the ATLAS collaboration, for the two considered benchmark points with masses $m(\tilde{\tau}, \tilde{\chi}_1^0) = (120, 1)$ and $(280, 1)$ GeV respectively. For each cut, we have calculated the related efficiency

$$\epsilon_i = \frac{n_i}{n_{i-1}} \tag{14}$$

where n_i and n_{i-1} correspond to the number of events after and before the considered cut respectively. On the other hand, we have also evaluated the differences between the MADANALYSIS 5 (ϵ_i(MA5)) and ATLAS (ϵ_i(ATLAS)) cut efficiencies through the quantity

$$\delta_i = \frac{\epsilon_i(\text{MA5}) - \epsilon_i(\text{ATLAS})}{\epsilon_i(\text{ATLAS})}. \tag{15}$$

(Need to mention that MA5 is weighted to have same yield of ATLAS at Baseline cut?)

We observe that for both scenarios, a good agreement is obtained at each step of the cutflow, with the exception of the last cut on the M_{T2} variable. For the $m(\tilde{\tau}, \tilde{\chi}_1^0) = (120, 1)$ GeV scenario, we hence obtain a disagreement of 30%–40% for both signal regions. In constrast, for the $m(\tilde{\tau}, \tilde{\chi}_1^0) = (280, 1)$ GeV scenario does not feature any strong issue at all, the two cutflow agreeing at the level of a few percent.

By lack of additional publicly available experimental information, we have not been able to investigate this issue at a very deep level. We have nevertheless compared M_{T2} distributions as predicted by MADANALYSIS 5 after all cuts, to those released by the ATLAS collaboration.[6] We have considered the two signal regions and both scenarios. Our results are shown in Fig. 2.

We observe that the global shape of the distribution is generally well reproduced, although the curves exhibit large differences that explain our findings at the level of the cutflow tables. However, one must note that the differences concern cases where a not so large number of (unweighted) events survive. Large Monte Carlo uncertainties of 10%–20% of percent are thus expected, both for our predictions and the ATLAS results.

On different lines, the number of signal events after all cuts are in the same ballpark, so that the potential impact on limit setting is mild. For this reason, the

Table 2. Cut-flow associated with a simplified model benchmark scenario defined by $m(\tilde{\tau}, \tilde{\chi}_1^0) = (120, 1)$ GeV and for the $pp \to \tilde{\tau}\tilde{\tau}$ production process. We compare ATLAS official results and MadAnalysis 5 predictions through the expected number of events after each cut and the corresponding efficiencies, and indicate their difference δ.

	ATLAS ($N_{weighted}$)	$\epsilon_i(\%)$	MA5 ($N_{weighted}$)	$\epsilon_i(\%)$	diff.(%)
$\tilde{\tau}\tilde{\tau}$ production with $m(\tilde{\tau}, \tilde{\chi}_1^0) = (120, 1)$ GeV					
Baseline cut	1686.80	-	1686.80	-	-
SR-low Mass					
Trigger and offline cuts	390.46	23.15	410.01	24.31	5.01
2 medium τ (OS) and 3rd medium τ veto	256.01	65.57	269.37	65.70	0.20
b-jet veto	250.59	97.88	263.66	97.88	-0.00
Light lepton veto	250.12	99.81	263.66	100	0.19
Z/H-veto	248.93	99.52	262.14	99.42	-0.10
$75 < E_T^{miss} < 150$ GeV	85.70	34.43	89.90	34.30	-0.38
2 tight τ	60.19	70.23	62.93	70.00	-0.33
$|\Delta\phi(\tau,\tau)| > 0.8$	60.14	99.92	62.75	99.72	-0.20
$|\Delta R(\tau,\tau)| < 3.2$	54.73	91.00	57.10	90.99	-0.01
$m_{T2} > 70$ GeV	9.78	17.87	14.65	25.66	43.58
All	-	0.58	-	0.87	49.80
SR-high Mass					
Trigger and offline cuts	101.23	6.00	96.35	5.71	-4.82
2 medium τ (OS) and 3rd medium τ veto	67.04	66.23	63.23	65.62	-0.91
b-jet veto	63.98	95.44	60.37	95.47	0.04
Light lepton veto	63.87	99.83	60.36	99.99	0.16
Z/H-veto	58.33	91.33	55.70	92.28	1.04
≥ 1 tight τ	57.29	98.22	50.69	91.00	-7.35
$|\Delta\phi(\tau,\tau)| > 0.8$	56.71	98.99	49.99	98.63	-0.36
$|\Delta R(\tau,\tau)| < 3.2$	51.74	91.24	45.41	90.84	-0.43
$m_{T2} > 70$ GeV	7.18	13.88	8.24	18.14	30.75
All	-	0.43	-	0.49	14.76

good agreement for one of the two benchmarks and the global reproduction of the M_{T2} shapes for both scenarios, we consider this reimplementation as validated.

4. Conclusions

In this note, we detail our implementation of the ATLAS-SUSY-2018-04 search in the MadAnalysis 5 framework. Our analysis has been validated in the context of a supersymmetry-inspired simplified benchmark model in which the Standard Model is extended by a neutralino and a stau. Both stau chiralities are considered, as the stau is considered to decay into a tau lepton and a neutralino. Our validation relies

Table 3. Same as in Table 2 but for a scenario with supersymmetric masses $m(\tilde{\tau}, \tilde{\chi}_1^0) = (280, 1)$ GeV.

	ATLAS ($N_{weighted}$)	$\epsilon_i(\%)$	MA5 ($N_{weighted}$)	$\epsilon_i(\%)$	diff.(%)
$\tilde{\tau}\tilde{\tau}$ production with $m(\tilde{\tau}, \tilde{\chi}_1^0) = (280, 1)$ GeV					
Baseline cut	184.36	-	184.36	-	-
SR-low Mass					
Trigger and offline cuts	73.74	40.00	69.97	37.95	-5.12
2 medium τ (OS) and 3rd medium τ veto	47.86	64.90	46.23	66.08	1.81
b-jet veto	46.63	97.43	44.94	97.20	-0.24
Light lepton veto	46.49	99.70	44.94	99.99	0.30
Z/H-veto	44.84	96.45	43.83	97.54	1.13
$75 < E_T^{miss} < 150$ GeV	17.48	38.98	16.26	37.10	-4.83
2 tight τ	12.04	68.88	11.38	70.00	1.63
$|\Delta\phi(\tau,\tau)| > 0.8$	12.04	100	11.33	99.55	-0.45
$|\Delta R(\tau,\tau)| < 3.2$	11.08	92.03	10.35	91.32	-0.77
$m_{T2} > 70$ GeV	6.08	54.87	5.64	54.50	-0.68
All	-	3.30	-	3.06	-7.24
SR-high Mass					
Trigger and offline cuts	47.64	25.84	42.10	22.83	-11.64
2 medium τ (OS) and 3rd medium τ veto	30.72	64.48	27.80	66.03	2.40
b-jet veto	29.34	95.51	26.83	96.52	1.06
Light lepton veto	29.27	99.76	26.83	99.99	0.23
Z/H-veto	24.88	85.00	24.01	89.50	5.30
≥ 1 tight τ	24.21	97.31	21.85	91.00	-6.48
$|\Delta\phi(\tau,\tau)| > 0.8$	23.29	96.20	21.19	96.96	0.79
$|\Delta R(\tau,\tau)| < 3.2$	21.95	94.25	19.68	92.91	-1.42
$m_{T2} > 70$ GeV	14.35	65.38	13.37	67.91	3.88
All	-	7.78	-	7.25	-6.84

on two different benchmark points in the parameter space.

By comparing our predictions for different cutflows for the two benchmarks with the official ones provided by the ATLAS collaboration in Ref. [5], we have found an agreement at each step of the analysis, except for the last cut on the stranverse mass variable m_{T2} cut for the light stau scenario. While the shape of the distribution is correctly reproduced, large difference leads to a quite different cut efficiency. Due to the lack of more information, we have however not been able to investigate the issue more precisely.

As we got an agreement at the level of a few percent for the heavy stau scenario, and that the discrepancies for the light stau scenarios are connected with large Monte Carlo uncertainties (and are thus less significant), we have considered our
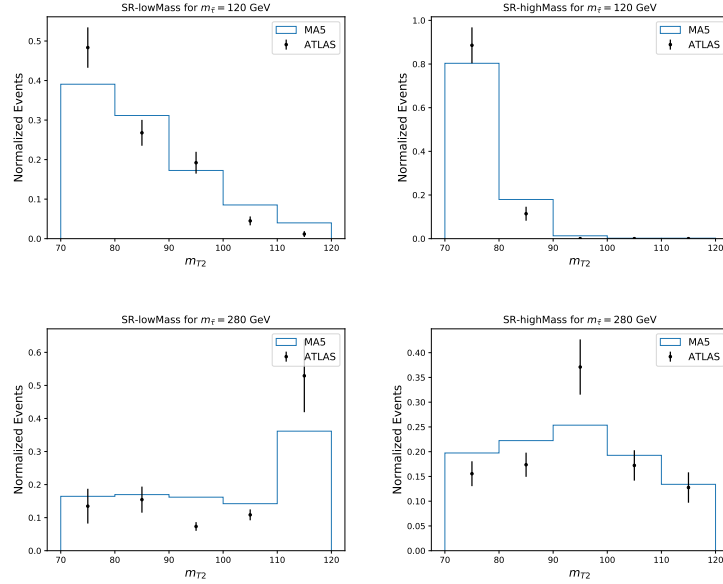
10 *Jongwon Lim, Chih-Ting Lu, Jae-hyeon Park and Jiwon Park*

Fig. 2.   The m_{T2} distributions after all cuts, for the SR-low Mass (left) and SR-high Mass (right) signal regions, and for the $m(\tilde{\tau}, \tilde{\chi}_1^0) = (120, 1)$ GeV (top panel) and $m(\tilde{\tau}, \tilde{\chi}_1^0) = (280, 1)$ GeV (bottom panel) scenarios.

reimplementation as validated. As a side remark, we emphasize that the differences would not lead to a significant impact for any limit setting procedure based on the light stau signal, the signal regions being here populated by a small number of events in both cases. (I don't get this side remark part. This might be ok for 120 GeV SR-highmass (considering systematic and statistical uncertainties), but low mass shows   50% difference. AFAIK limit is usually linearly depend on expected yield (or cross section), so if we have 50% more events at the end, we will have % higher limit. Please correct me if I'm wrong.)

References

1. E. Conte and B. Fuks, Int. J. Mod. Phys. A **33** (2018) no.28, 1830027 [arXiv:1808.00480 [hep-ph]].
2. B. Dumont *et al.*, Eur. Phys. J. C **75** (2015) no.2, 56 [arXiv:1407.3278 [hep-ph]].
3. E. Conte, B. Dumont, B. Fuks and C. Wymant, Eur. Phys. J. C **74** (2014) no.10, 3103 [arXiv:1405.3982 [hep-ph]].
4. E. Conte, B. Fuks and G. Serret, Comput. Phys. Commun. **184** (2013) 222 [arXiv:1206.1599 [hep-ph]].
5. G. Aad *et al.* [ATLAS Collaboration], Phys. Rev. D **101**, no. 3, 032009 (2020) doi:10.1103/PhysRevD.101.032009 [arXiv:1911.06660 [hep-ex]].
6. G. Aad *et al.* [ATLAS], doi:10.17182/hepdata.92006
7. M. Cacciari, G. P. Salam and G. Soyez, JHEP **0804**, 063 (2008) doi:10.1088/1126-6708/2008/04/063 [arXiv:0802.1189 [hep-ph]].
8. C.   Duhr   and

B. Fuks, Comput. Phys. Commun. **182**, 2404 (2011) doi:10.1016/j.cpc.2011.06.009 [arXiv:1102.4191 [hep-ph]].

9. A. Alloul, N. D. Christensen, C. Degrande, C. Duhr and B. Fuks, Comput. Phys. Commun. **185**, 2250 (2014) doi:10.1016/j.cpc.2014.04.012 [arXiv:1310.1921 [hep-ph]].

10. J. Alwall *et al.*, JHEP **1407**, 079 (2014) doi:10.1007/JHEP07(2014)079 [arXiv:1405.0301 [hep-ph]].

11. R. D. Ball, V. Bertone, S. Carrazza, C. S. Deans, L. Del Debbio, S. Forte, A. Guffanti, N. P. Hartland, J. I. Latorre and J. Rojo, *et al.* Nucl. Phys. B **867**, 244-289 (2013) doi:10.1016/j.nuclphysb.2012.10.003 [arXiv:1207.1303 [hep-ph]].

12. M. L. Mangano, M. Moretti, F. Piccinini and M. Treccani, JHEP **0701**, 013 (2007) doi:10.1088/1126-6708/2007/01/013 [hep-ph/0611129].

13. J. Alwall, S. de Visscher and F. Maltoni, JHEP **0902**, 017 (2009) doi:10.1088/1126-6708/2009/02/017 [arXiv:0810.5350 [hep-ph]].

14. T. Sjostrand, S. Mrenna and P. Z. Skands, Comput. Phys. Commun. **178**, 852 (2008) doi:10.1016/j.cpc.2008.01.036 [arXiv:0710.3820 [hep-ph]].

15. J. de Favereau *et al.* [DELPHES 3 Collaboration], JHEP **1402**, 057 (2014) doi:10.1007/JHEP02(2014)057 [arXiv:1307.6346 [hep-ex]].

16. M. Cacciari, G. P. Salam and G. Soyez, Eur. Phys. J. C **72**, 1896 (2012) doi:10.1140/epjc/s10052-012-1896-2 [arXiv:1111.6097 [hep-ph]].

17. ATLAS Collaboration, ATLAS-CONF-2017-029.

18. C. G. Lester and D. J. Summers, Phys. Lett. B **463**, 99-103 (1999) doi:10.1016/S0370-2693(99)00945-4 [arXiv:hep-ph/9906349 [hep-ph]].

19. H. C. Cheng and Z. Han, JHEP **12**, 063 (2008) doi:10.1088/1126-6708/2008/12/063 [arXiv:0810.5178 [hep-ph]].

20. C. Degrande, C. Duhr, B. Fuks, D. Grellscheid, O. Mattelaer and T. Reiter, Comput. Phys. Commun. **183**, 1201-1214 (2012) doi:10.1016/j.cpc.2012.01.022 [arXiv:1108.2040 [hep-ph]].

21. T. Sjöstrand, S. Ask, J. R. Christiansen, R. Corke, N. Desai, P. Ilten, S. Mrenna, S. Prestel, C. O. Rasmussen and P. Z. Skands, Comput. Phys. Commun. **191**, 159-177 (2015) doi:10.1016/j.cpc.2015.01.024 [arXiv:1410.3012 [hep-ph]].

22. ATLAS Collaboration, ATL-PHYS-PUB-2014-021.